Mechanisms of forced tropical meridional energy flux change

Spencer A. Hill, *

Program in Atmospheric and Oceanic Sciences, Princeton University, Princeton, NJ

Yi Ming and Isaac M. Held

Geophysical Fluid Dynamics Laboratory/NOAA, Princeton, NJ

* *Corresponding author address:* Spencer Hill, NOAA Geophysical Fluid Dynamics Laboratory, 201 Forrestal Rd, Princeton, NJ 08540.

E-mail: spencerh@princeton.edu

ABSTRACT

By altering the mean and spatial pattern of sea surface temperatures (SSTs), anthropogenic greenhouse gases and aerosols modulate the meridional transport of energy by the tropical atmosphere. This energy flux varies seasonally in the climatology – in total, its partitioning among the Hadley cells and eddy components, and, for the Hadley cells, the relative importance of the mass flux and the gross moist stability (GMS) – suggesting that forced anomalies will also vary seasonally. We investigate this behavior using an atmospheric general circulation model forced with SST anomalies representative of the equilibrium response to historical emissions of either forcing agent, the tropical mean SST anomaly applied uniformly, or the full SST anomalies minus the tropical mean.

Greenhouse gases increase poleward energy transport year-round via mean warming, but this is partially counteracted by their polar amplified spatial pattern. Aerosols induce strong northward energy flux anomalies in the deep tropics, which manifest primarily in the Hadley cells and that stem from the northern hemisphere (NH) cooling relative to the southern hemisphere (SH). Greenhouse gases weaken the Hadley cell mass flux throughout the annual cycle, with contributions from both mean and spatial pattern components. Aerosols strengthen NH cell and weaken SH cell circulation, again due to the spatial pattern of relative NH cooling. We create a perturbation theory for GMS based on a previous simple estimate of GMS as the difference between surface moist static energy locally and at the Intertropical Convergence Zone (ITCZ). Our theory, which invokes a thermodynamic scaling argument for the moisture term, captures the qualitative GMS behavior throughout the seasonal cycle in most of the simulations. The estimate suggests that the GMS response is tied to the meridional profile of SST change in the tropics acting on the climatological moisture profile. We discuss the theory's relevance to forced ITCZ shifts in which changes in moisture convergence are large.

1. Introduction

Earth absorbs more solar radiation near the equator than at the poles, driving atmospheric circulations that transport energy poleward in both the northern and southern hemispheres (NH and SH). This poleward flux manifests through the mean meridional circulation (MMC), stationary eddies, and transient eddies. Symbolically,

$$[\overline{mv}] = \underbrace{[\overline{m}][\overline{v}]}_{\text{MMC}} \quad + \quad \underbrace{[\overline{m}^*\overline{v}^*]}_{\text{stationary eddies}} \quad + \quad \underbrace{[\overline{m'v'}]}_{\text{transient eddies}}, \tag{1}$$

where $m = c_p T + gz + L_v q$ is moist static energy (MSE), overbars denote time means, primes denote deviations from the time mean, square brackets denote zonal means, and asterisks denote deviations from the zonal mean. In the tropics, the MMC consists of the two Hadley cells. Note that moist static energy neglects kinetic energy, which is rarely important for large-scale energy transport.

Both the total atmospheric energy transport and its partitioning among these flow components vary with the seasonal cycle in the tropics (e.g. Trenberth and Stepaniak 2003). The Hadley cells dominate the energy transport in the deep tropics and primarily flux energy poleward, though the large cross-equatorial cell during the solsticial seasons[1] includes a flux from the summer to the winter hemisphere. Stationary eddy transports are also primarily poleward. Transient eddy poleward fluxes are large in autumn and winter, increasing in magnitude moving away from the equator. The dynamics controlling the Hadley cells' strength and extent is also seasonal, with the winter cell largely adhering to the classical angular momentum conserving models (e.g. Held and Hou 1980) but with eddy stresses strongly affecting the mass circulation in the equinoctial and summer cells and the poleward flank of the winter cell (e.g. Held 2001a; Walker and Schneider 2006; Merlis et al. 2013a).

The fluxes of energy and mass by the Hadley cells are linked via the gross moist stability (GMS). As the Hadley cells overturn, their upper and lower branches transport energy in

[1] This cell is variously referred to as the "winter", "cross-equatorial", "solsticial", or "monsoonal" cell in the literature.

opposite directions, so the net meridional energy flux depends on their degree of compensation (Held and Hoskins 1985). This compensation itself depends on two factors – (1) the rate of mass circulation (which, following convention, we refer to as the "mass flux") and (2) the meridional energy flux per unit mass flux, which is the GMS. Symbolically at a given latitude ϕ,

$$F_{\mathrm{HC}}(\phi) = \Psi_{\max}(\phi)\Delta_{\mathrm{HC}}(\phi), \tag{2}$$

where F_{HC} is the energy flux by the Hadley cells, $\Psi_{\max}$ the mass flux, and Δ_{HC} the GMS. This expression in fact defines GMS as the ratio of the Hadley cell energy flux to the mass flux.[2] GMS can be thought of as the "efficiency" of meridional energy transport by the Hadley cells, since it indicates the amount of energy flux per unit mass flux.

It follows from Eq. 2 (for sufficiently small perturbations) that fractional changes in these quantities are related by

$$\frac{\delta F_{\mathrm{HC}}(\phi)}{F_{\mathrm{HC}}(\phi)} = \frac{\delta\Psi_{\max}(\phi)}{\Psi_{\max}(\phi)} + \frac{\delta\Delta_{\mathrm{HC}}(\phi)}{\Delta_{\mathrm{HC}}(\phi)}. \tag{3}$$

Meridionally asymmetric energy perturbations – e.g. the NH-centric anthropogenic aerosols or asymmetric feedbacks to the more uniform greenhouse gas forcing – can push the inner boundary of the Hadley cells, and with it the intertropical convergence zone (ITCZ), away from the energy deficient hemisphere (e.g. Kang et al. 2008, 2009; Ming and Ramaswamy 2011; Chiang and Friedman 2012; Frierson and Hwang 2012). This meridional shift manifests as a spin up of the cell in the energy excessive hemisphere and a spin down in the energy deficient one. But if GMS change compensates for some of the induced energy imbalance, then by Eq. 3 the mass circulation response – and with it the ITCZ shift – will be weaker.

[2] The HC subscript on the gross moist stability term is meant to emphasize that the energy flux is by the Hadley cells only. The analogous quantity that also includes eddy energy transports is known as "total GMS" (e.g. Kang et al. 2009). Moreover, gross moist stability can be defined in other ways than the zonal-mean, meridional flux form we use here, such as using the flux divergence (e.g. Neelin and Held 1987) or vertical velocity profile (e.g. Chou et al. 2009), in which cases it is a function of both longitude and latitude. But all forms are conceptually a measure of the column's susceptibility to moist convection.

Merlis et al. (2013a) show that, in an intermediate complexity aquaplanet model, GMS can actually overcompensate for an imposed meridional energy imbalance due to orbital precession, such that the fractional mass flux change is the opposite sign of the fractional energy flux change. Merlis et al. (2013a) also find the GMS response to be well captured by a simple approximation by Held (2001b) relating GMS to the surface meridional moist static energy gradient.

Several other recent studies have investigated GMS in the context of meridional energy transports and movement of the ITCZ (e.g. Frierson 2007; Kang et al. 2009; Kang and Held 2012; Merlis et al. 2013b,c), but all use zonally symmetric aquaplanet models (or with a simple zonally symmetric NH continent in Merlis et al. (2013b)), often with simplified treatments of radiation, convection, and other relevant processes. The behavior of tropical moist stability in global warming has also been studied more generally, with stability changes fundamental to the "upped-ante" mechanism of Neelin et al. (2003) and the "rich-get-richer" mechanism of Chou and Neelin (2004).

The role of surface temperatures in tropical dynamics has long been appreciated. The ITCZ in axisymmetric models is co-located with the near-surface MSE maximum (Privé and Plumb 2007), itself strongly dependent on surface temperatures. Deep convection in the ITCZ effectively communicates surface conditions all the way to the tropopause and nearly homogenizes the column MSE (Held 2001b). The weak temperature gradient constraint aloft (e.g. Sobel et al. 2001) can then effectively communicate this to the whole tropical free troposphere. Moreover, anthropogenic forcing can alter the tropical circulation and precipitation via changing the mean (e.g. Held and Soden 2006) and spatial pattern (e.g. Xie et al. 2013) of SSTs.

These considerations compel us to study how anthropogenically forced changes to the SST field – both its mean and its spatial pattern – alter the tropical meridional energy flux throughout the seasonal cycle in a comprehensive atmospheric general circulation model (AGCM). We force the AGCM with SST anomalies induced by either historical anthropogenic well-mixed greenhouse gases or aerosols, the tropical mean SST anomalies applied everywhere, or the full SST anomalies minus their tropical mean. Section 2 describes our methodology, with additional details in the Appendix. Section 3 describes the results of these prescribed SST simulations. Discussion and summary follow in Sections 4 and 5, respectively. We view these simulations as a bridge between the aforementioned idealized aquaplanet simulations and fully coupled GCMs (or the real world) in which such a decomposition into mean and spatial pattern components is not feasible.

2. Methods

We first create SST anomalies representative of the effects of either forcing agent using the experiments of Ming and Ramaswamy (2009) with the Geophysical Fluid Dynamics Laboratory (GFDL) AM2.1 AGCM (GFDL Atmospheric Model Development Team 2004; Delworth et al. 2006) coupled to a 50 meter mixed-layer (or "slab") ocean. This configuration is referred to as SM2.1. AM2.1 is modified from its standard formulation to account for the aerosol indirect effects by incorporating a prognostic cloud droplet number concentration scheme for shallow cumulus and stratiform clouds that depends on local aerosol concentrations (Ming et al. 2006, 2007). A control case with pre-industrial atmospheric composition is perturbed either with pre-industrial to present day well-mixed greenhouse gas or aerosol burdens. We run the pre-industrial control, present day greenhouse gases, and present day aerosol cases to equilibrium, averaging the annual cycle of SSTs over model years 61–80 to produce a climatological SST annual cycle. We then subtract the control from the perturbation SSTs to obtain an SST anomaly field for each forcing agent.

We then add these SST anomalies to observed climatological SSTs from the HadISST observational dataset (Rayner et al. 2003) averaged over 1980–2005, again retaining an annual cycle. These SST fields along with observed climatological sea ice are then used to drive AM2.1, with the same annual cycle repeated each year. This yields a control case and greenhouse gas and aerosol perturbation cases. The AGCM is run for 17 years, the first year discarded as spin-up and results averaged over the subsequent 16. Results averaged over the first 8 years or subsequent 8 years of the averaging period are largely similar to results using all 16.

Importantly, the atmospheric composition in all prescribed SST experiments is present day, to be consistent with the climatological SSTs from HadISST upon which the anomalies are added. Therefore, any differences in the climate response stem solely from differences in the imposed SST fields. There are no prescribed surface fluxes.

To discern the roles of changes to the mean vs. spatial pattern of SSTs, we create two additional simulations for each forcing agent. In the first, the annual mean SST change averaged over the tropics (+2.0 K for greenhouse gases, −1.1 K for aerosols; tropics defined as 30°S–30°N) is added to the climatology at every ocean gridpoint and timestep.[3] In the second, this tropical mean SST change is subtracted from the full SST anomaly field at each ocean gridpoint before being added to the climatology. These experiments thus represent the mean temperature change and spatial pattern components, respectively. The spatial pattern cases are analogous to the "relative SST" concept introduced by Vecchi and Soden (2007) used to study hurricane behavior. Ma and Xie (2013) perform an analogous decomposition into mean and spatial pattern components in the CAM3 AGCM in their analysis of circulation and precipitation responses to anthropogenic forcing.

The tropical mean temperature change was chosen so that the spatial pattern simulations would have zero mean SST change in the tropics, thereby negating any change in atmospheric specific humidity induced via the Clausius-Clapeyron relation. Indeed, changes in annual and tropical mean water vapor path are −0.1 and −0.2 kg m^{-2} for the spatial pattern cases of greenhouse gases and aerosols, respectively, compared to +6.9 and −3.2 kg m^{-2} for the mean temperature change components and +6.7 and −3.4 kg m^{-2} for the full perturbation

[3]By coincidence of the tropical mean greenhouse gas warming being just under 2 K, the mean warming case is essentially identical to commonly run "plus 2 K" or "Cess" uniform SST warming simulations.

cases. In this sense, the mean and spatial pattern cases can be roughly thought of as the "thermodynamic" and "dynamic" components of the total response. The atmosphere responds quite linearly to the mean/spatial pattern decomposition, in that for all quantities analyzed the response to the full perturbation roughly equals the sum of the responses in the corresponding mean temperature change and spatial pattern cases (shown below for the energy flux).

The Appendix describes in detail how the energy flux, mass flux, and gross moist stability are calculated, including the partitioning of the energy flux among the MMC, stationary eddy, and transient eddy terms, a simple adjustment based on mass balance considerations applied in the MMC energy flux computation, and the sensitivity of the energy flux calculations to the height of the vertical integral.

3. Results

a. Surface temperature

Fig. 1 shows the annual mean latitude-longitude pattern of surface air temperature change for the full and spatial pattern perturbation cases of both forcing agents. Tight coupling of the ocean and near-surface atmosphere cause these values over ocean to be nearly identical to the imposed SSTs (not shown), except for high latitude locations where the prevailing meteorology decouples the atmosphere from the surface. Table 1 lists some pertinent annual mean quantities averaged over different regions. The mean warming by greenhouse gases and weaker cooling by aerosols are evident (+2.1 and −1.2 K in the global mean, respectively), as are the polar amplified spatial pattern of the greenhouse gases and the aerosol-induced cooling of the NH relative to the SH (NH and SH mean SST change are +2.2 and +2.0 K respectively for greenhouse gases and −1.6 and −0.9 K for aerosols).

Fig. 1 also shows the annual cycle of the zonal mean surface air temperature change for both full cases. The weakest changes occur in the Arctic during NH summer, when melting ice and snow peg surface temperature to the freezing point. Both also have their maximum magnitudes in the Arctic winter, as the prevailing near surface inversion inhibits turbulent fluxes and thus the energetic anomalies must be shed via changes in longwave emission (e.g. Boé et al. 2009; Lesins et al. 2012). This results in seasonal variations in the NH high latitude surface temperature response of ∼6 K for greenhouse gases and ∼4 K for aerosols, in contrast to $\lesssim$1 K in the tropics for either forcing agent.

b. *Energy flux*

Fig. 2 shows the annual cycle of the monthly mean meridional energy flux in total and for the three flow components in the control experiment. Outside ∼20°S–20°N, transport is poleward in both hemispheres year-round, reaching peak magnitudes near 7 PW in the mid-latitudes in early winter. The Hadley cells contribute up to ∼3 PW in mid- to late winter of either hemisphere. Stationary eddies contribute up to ∼3 PW to the poleward transport in the NH mid-latitudes in winter, but their contribution in the tropics is weaker in both hemispheres. Transient eddies contribute more than 5 PW to the poleward energy transport in autumn and winter over much of the mid latitudes, with spillover of up to 4 PW extending through the tropics in these seasons.

Overlaid on the color contours in this and subsequent figures are grey curves denoting the locations of the Hadley cells' poleward boundaries and their shared interior boundary. These are calculated as the zero crossings of the 500 hPa meridional mass streamfunction estimated using linear interpolation between the grid latitudes at which the streamfunction changes sign.[4] As Dima and Wallace (2003) demonstrate for reanalysis data, the two cells smoothly vary throughout the year between "equinoctial" and "solsticial" patterns (rather than displaying "square wave" behavior dominated by the solsticial cell as had been previ-

[4]Results are insensitive to other commonly used definitions of the poleward boundaries, e.g. where the 500 hPa streamfunction reaches 10% of its maximum value within the Hadley cells or where the streamfunction at its level of maximum reduces to 10% of that maximum.

ously posited).

Fig. 3 shows the total anomalous energy flux and the contributions of each flow component for the full greenhouse gas and aerosol experiments, with overlaid grey contours marking the Hadley cell boundaries of the perturbation run. Greenhouse gases increase poleward transport for most months/latitudes, with maximum magnitudes just under 0.4 PW. This is driven by eddies, with stationary eddies contributing northward anomalies over much of the NH tropics and transient eddies enhancing poleward energy transport over most of the extratropics of both hemispheres. In contrast, the Hadley cells tend to oppose this enhanced poleward transport, contributing southward anomalies in the NH winter cell up to -0.6 PW and northward anomalies in the SH winter cell up to $+0.4$ PW.

Aerosols yield northward anomalies in the deep tropics year-round. They are centered on the equator, reach $+0.7$ PW in the SH winter cell, and manifest almost exclusively via the Hadley cells. Interestingly, in the NH they are strongest in summer when Arctic cooling is minimum, rather than winter when the meridional gradient in temperature change is largest. Outside this region of strong northward anomalies, the picture is generally reduced poleward flux, with equatorward anomalies in either hemisphere. Stationary eddies contribute substantially to this weakening in the SH tropics, while transient eddies drive the extratropical response.

Some latitudes and months exhibit pronounced re-partitioning among the flow components despite weak change in the total flux. For example, the strongest anomalies in any of the fields are for the aerosol transient eddies in February in the NH mid-latitudes, with values reaching -0.8 PW. However, moderate northward anomalies in both the MMC and stationary eddy fields compensate, resulting in only a -0.1 PW anomaly in the total flux. Analogous behavior can be discerned at other latitudes/months.

Fig. 4 shows the change in total atmospheric energy transport for the mean and spatial pattern cases of each forcing agent and their sum. For greenhouse gases, these components oppose each other at most latitudes throughout the annual cycle. The mean warming enhances poleward energy transport via increased poleward moisture transport (not shown) (Held and Soden 2006; Hwang and Frierson 2010), with magnitudes near 0.3 PW for much of the year in the subtropics. In contrast, the polar amplified spatial pattern reduces the meridional temperature gradient, thereby weakening the poleward flux. The former effect being stronger than the latter in this case, the net result is enhanced poleward energy transport that is weaker than the mean warming case (Caballero and Langen 2005).

Aerosol mean cooling weakens the poleward energy flux by more than 0.2 PW at most latitudes/months via the same moisture flux mechanism (albeit with opposite sign) as the greenhouse gas mean warming case. Meanwhile, the aerosol spatial pattern drives the strong northward anomalies (up to +0.7 PW) in the deep tropics apparent in the full case. These anomalies are strongest just poleward of the Hadley cells' interior boundary in either hemisphere. Thus the mean and spatial pattern effects buttress one another in the southern Hadley cell but oppose each other in the northern cell. The net result is northward anomalies in the full aerosol case that peak in the SH winter cell just south of the cells' shared border.

Combining these two decompositions – into MMC/stationary eddy/transient eddy components of the energy flux and into mean/spatial pattern of SSTs – the following picture emerges: greenhouse gas warming enhances poleward energy transport mostly through eddies, an effect that is partially negated by the weakened meridional temperature gradient. Meanwhile, the aerosol spatial pattern of NH cooling relative to the SH induces northward anomalies in the deep tropics that manifest via the Hadley cells and that are superimposed on reduced poleward energy transport due to the mean cooling. Comparing the sum of the mean and spatial pattern components (Fig. 4e,f) to the full case (Fig. 3a,b) reveals that the response is quite linear to the imposed decomposition for either forcing agent.

c. *Mass flux*

That the Hadley cells contribute non-negligibly for greenhouse gases and substantially for aerosols to the anomalous energy flux justifies analysis of the relative roles of both the mass flux and gross moist stability, starting with the mass flux. Following convention, we define the mass flux, denoted $\Psi_{\mathrm{max}}(\phi)$, at each latitude as the signed maximum magnitude of the Eulerian mean meridional streamfunction, where

$$\Psi(\phi, p) = 2\pi a \cos\phi \int_0^p [\,\overline{v}\,]\, \mathrm{d}p/g. \tag{4}$$

With this sign convention, positive values correspond to northward flow aloft and southward flow in the surface branch as in the NH cell; all subsequent references to northward or southward mass flux anomalies refer to flow in the upper branch. For either cell in the climatology, Ψ_{max} is of the same sign as the energy flux, F_{HC}.

Fig. 5 shows the mass flux annual cycle in the control for 45°S-45°N. Peak magnitudes occur in the solsticial seasons in the winter cell. It is strongly seasonal in the deep tropics, at the equator ranging from 15×10^{10} kg s^{-1} in January to -24×10^{10} kg s^{-1} in July. This seasonality weakens moving towards the subtropics: at 30° in either hemisphere the mass flux is of the same sign year-round, with its maximum and minimum monthly values differing only by around $4{\times}10^{10}$ kg s^{-1}. Values drop off sharply poleward of the Hadley cells.

Fig. 6 shows the mass flux response annual cycle in the six perturbation experiments. Interestingly, changes of substantial magnitude are bounded by the extent of the Hadley cells interior boundary seasonal migration, ∼15°S–15°N. This suggests that the Hadley circulation response manifests primarily via alterations to its interior boundary location. For greenhouse gases the interior boundary moves southward April through September and northward otherwise, while for aerosols it moves southward year-round – in both cases agreeing with the sign of the mass flux changes.

For greenhouse gases, the mass flux anomalies vary seasonally as to oppose the climatology, being southward in the northern winter cell up to -5.4×10^{10} kg s^{-1} and northward in the southern winter cell up to 3.6×10^{10} kg s^{-1}. Kang et al. (2013) likewise see weakening of both winter cells in a 40-member ensemble of the CCSM4 GCM subject to A1B emissions scenario radiative forcing (which is dominated by increased greenhouse gas concentrations).

Coincidentally, the mass flux responds similarly to the mean warming and spatial pattern components of greenhouse gases, both acting primarily against the climatology (albeit less than the full case). For mean warming, this is a well known result stemming from specific humidity increasing faster than precipitation with temperature, such that the tropical convective mass flux must weaken (Held and Soden 2006). For the polar amplified spatial pattern, the reduced meridional temperature gradient necessitates weaker poleward energy fluxes as discussed above. This is partly accomplished in the deep tropics via a weakening of the mass flux in the winter cell. The net result of these two distinct but complementary mechanisms is a stronger weakening of the circulation in total for greenhouse gases than for either the mean or spatial pattern component alone.

Aerosols induce strong northward anomalies nearly year-round in the deep tropics, with maximum values in January through March near 6×10^{10} kg s^{-1}. These strong anomalies counteract the climatology in the NH cell and reinforce it in the SH cell amd are co-located with the strong northward energy flux anomalies (Fig. 3). In other words, ignoring changes to gross moist stability (discussed below) a moment, the spin up of the NH cell enhances the climatological northward energy flux while the spin down of the SH cell weakens the climatological southward energy flux in that cell. In both cases the anomalous energy flux is northward.

The mean cooling contributes weakly to this pattern, with substantial southward anomalies (up to -3.4×10^{10} kg s^{-1}) only in July through September just south of the boundary between the two Hadley cells. Whereas the greenhouse gas mean warming spins down the tropical circulation (discussed above), the mean cooling of aerosols does not appear to spin-up the circulation. On the one hand, aerosol cooling is of smaller magnitude than the greenhouse gas warming, and thus one would expect a weaker circulation response. On the other hand, the two responses are not simply scaled mirror images of each other. This behavior is still under investigation. Wyant et al. (2006) demonstrate asymmetric tropical changes in both shortwave and longwave cloud radiative forcings in plus-2K and minus-2K experiments conducted in AM2.1, which they attribute to differing condensate responses in regions of ascent. Interestingly, such asymmetry is absent in another AGCM (namely NCAR CAM3.0).

Nevertheless, the mean temperature change component contributes only weakly to the total aerosol mass flux response. Instead, the spatial pattern component drives the southward anomalies. This is consistent with the northward energy flux anomalies (Fig. 3) being driven by the Hadley cells of the spatial pattern component as well.

d. Gross moist stability

As explained in detail in the Appendix, we use a definition of GMS that includes only the Hadley cell contribution to the meridional energy flux, in order to understand the Hadley cell energy flux changes that dominate the total transport change for aerosols and counter-intuitively largely oppose the enhanced poleward energy transport by eddies for greenhouse gases.

1) Theory

We start with a simple estimate for GMS made by Held (2001b) (hereafter H01). GMS as defined by Eq. A5 is mathematically equivalent to a meridional flow-weighted difference between upper and lower level MSE (Neelin and Held 1987). In the limit of equal magnitude mass flow confined to one upper and one lower boundary layer, the mass flux weighting drops out and this simplifies to the upper minus lower level MSE. At the ITCZ, deep convection homogenizes MSE vertically. Additionally, the weak temperature gradient dynamical constraint in the free troposphere horizontally homogenizes temperature and geopotential fields aloft. Together these imply that the surface MSE at the ITCZ sets the MSE field aloft throughout the tropics, and therefore GMS at a given latitude within the Hadley cells depends on the difference between surface MSE values locally and at the ITCZ:

$$\Delta_{\mathrm{HC}}(\phi) \approx m_{\mathrm{ITCZ}} - m(\phi), \tag{5}$$

where the subscript ITCZ denotes the value at the latitude of the ITCZ and all variables refer to surface values.

H01 further simplifies by noting that geopotential is zero at the surface and writing $q = \mathcal{H} q_s$, where $\mathcal{H}$ and q_s are relative humidity and saturation specific humidity respectively, such that $m = c_p T + L_v \mathcal{H} q_s$. Then, neglecting meridional variations in $\mathcal{H}$, GMS becomes

$$\Delta_{\mathrm{HC}}(\phi) \approx \left(c_p + L_v \overline{\mathcal{H}} \frac{\mathrm{d}q_s}{\mathrm{d}T} \right) (T_{\mathrm{ITCZ}} - T(\phi)), \tag{6}$$

where $\overline{\mathcal{H}}$ is the tropical mean relative humidity and $\mathrm{d}q_s/\mathrm{d}T$ is set by the Clausius-Clapeyron relation. Eq. 6 states that the gross moist stability is determined solely by the meridional profile of surface temperatures and the tropical mean surface relative humidity, since temperature also sets the saturation specific humidity via Clausius-Clapeyron. While H01 is concerned with the climatological annual mean GMS, Eqs. 5 and 6 are easily modified to represent GMS changes in time, e.g. between perturbation and control experiments. Merlis et al. (2013a) do so using Eq. 5, finding it to be a useful approximation of the GMS response to orbital precession in an idealized aquaplanet GCM (their Fig. 9).

We do likewise for our simulations but using a modified form of Eq. 6. Variations of relative humidity with latitude in the tropics tend to exceed those at a given latitude with time. For example, annual and zonal mean relative humidity at 2 m above the surface varies by $\sim$15% from the equator to 30° in either hemisphere in our control simulation, whereas the maximum magnitude change at a given tropical latitude from the control to any perturbation simulation is $\sim$1%. Therefore, we retain meridional variations in relative humidity and instead assume that specific humidity obeys a simple thermodynamic scaling relation (c.f. Held and Soden 2006), i.e. $\delta q/q = \alpha \delta T$, where $\alpha = 0.07\%\ \mathrm{K}^{-1}$ represents the fractional increase in saturation vapor pressure with temperature via Clausius-Clapeyron. Such a scaling of surface moisture also neglects changes in moisture convergence (i.e. “dynamical” change). Doing so results in the following approximation for GMS change:

$$\delta\Delta_{\mathrm{HC}}(\phi) = (c_p + \alpha L_v q_{\mathrm{ITCZ}})\delta T_{\mathrm{ITCZ}} - (c_p + \alpha L_v q(\phi))\delta T(\phi), \tag{7}$$

where δ denotes the difference between two climate states. Rearranging terms reveals the condition governing the sign of GMS change (the two equalities can be replaced with either $>$ or $<$):

$$\delta\Delta_{\mathrm{HC}}(\phi) = 0 \quad \Longleftrightarrow \quad \frac{\delta T(\phi)}{\delta T_{\mathrm{ITCZ}}} = \frac{c_p + \alpha L_v q_{\mathrm{ITCZ}}}{c_p + \alpha L_v q(\phi)}. \tag{8}$$

Assuming that $q_{\mathrm{ITCZ}} > q(\phi)$, the right hand side of Eq. 8 is strictly greater than unity. Thus for GMS to remain constant, the magnitude of surface temperature change locally must exceed that at the ITCZ to an extent that depends on the existing specific humidity difference between them. Fig. 8 shows this ratio $\delta T(\phi)/\delta T_{\mathrm{ITCZ}}|_{\delta\Delta_{\mathrm{HC}}=0}$ for the control experiment. As zonal mean specific humidity decreases monotonically away from the ITCZ into the subtropics (not shown), the temperature change ratio increases monotonically, reaching $\sim$1.6 near the poleward boundaries of either Hadley cell.

For the particular case of a uniform δT, Eq. 8 reduces to $\delta\Delta_m(\phi) = \alpha L_v(q_{\mathrm{ITCZ}} - q(\phi))\delta T$. Again assuming $q_{\mathrm{ITCZ}} > q(\phi)$, the sign of the GMS change depends solely on the sign of δT. Uniform warming increases, and uniform cooling decreases, GMS at all latitudes outside the ITCZ, with the magnitude of the change increasing with the magnitude of the temperature change and moving towards the subtropics. Given that climatologically GMS also increases meridionally away from ITCZ, this behavior in the case of uniform warming can be thought of as another manifestation of “rich-get-richer” (Chou and Neelin 2004; Held and Soden 2006; Chou et al. 2009) behavior: the stable get stabler (taking liberty to define “the stable” as all latitudes outside the ITCZ.)

2) Results

Fig. 7 shows the annual cycle of GMS in the control simulation. All GMS plots absorb a $1/c_p$ factor as standard to get units of Kelvin and have values outside of the Hadley cells masked. Overlaid in the blue dotted curve is the ITCZ location, defined as the latitude of maximum zonal mean precipitation, linearly interpolated from the model grid to the point where $\partial P/\partial\phi = 0$. The control GMS qualitatively adheres to the H01 picture. It is near zero following the boundary separating the Hadley cells in its seasonal migration and increases nearly monotonically moving meridionally away, with values near 30 K at the poleward boundary of either Hadley cell. However, the ITCZ is displaced equatorward by several degrees latitude of the GMS minimum and Hadley cells shared border most of the year (Donohoe et al. 2013).

We discuss the aerosol simulations first, because the GMS response is simpler than for greenhouse gases. Fig. 9 shows the GMS response for the three aerosol cases and their corresponding estimates using Eq. 7. Values within 6° latitude of the Hadley cells' interior border on either side are masked out for the full calculation, as it becomes problematic near where the mass flux goes to zero. The theoretical estimate uses values at 925 hPa. Given its simplicity, Eq. 7 captures well the qualitative behavior throughout the seasonal cycle in each simulation. For the full and spatial pattern cases, aerosols decrease GMS in the southern Hadley cell and increase it in the northern cell for most of the year. For the uniform cooling case, the estimate features nearly monotonically decreasing GMS moving meridionally away from the convection zone. The simulated response to uniform cooling also predominantly features reductions, with notable exceptions in the NH summer cell and over much of the year for 15°S-30°S.

The spatial pattern component can also be understood via the theoretical estimate. Because zonal mean surface temperature change decreases (that is, becomes more negative) essentially monotonically moving northward, GMS will decrease at latitudes south of the ITCZ and increase at latitudes north based on Eq. 8. This response yields an anomalous northward MSE transport that acts against the imposed cooling of the NH relative to the SH. So as was the case with the MSE flux $F_{\mathrm{HC}}(\phi)$, the aerosol mean cooling and spatial pattern components reinforce each other in the southern Hadley cell and counteract each other in the northern cell, resulting in generally weaker increases in the northern cell than decreases in the southern cell for the full aerosol case.

Table 2 lists for the full aerosol simulation each month the change in F_{HC} and the fractional changes in F_{HC}, $\Psi_{\max}$, and Δ_{HC} at the latitude of the maximum magnitude of $\Psi_{\max}$, $\phi_{\max}$, which is essentially the center of the stronger Hadley cell. In all months in which the SH cell is stronger (April through October), more than half of the energy flux fractional change manifests via GMS, whereas the converse holds in the NH cell (November through March). This includes the NH monsoon season (JJA), during which precipitation over the Indian and East Asian monsoon regions drops markedly in the aerosol full and spatial pattern simulations (not shown) due to the hemispheric imbalance (Bollasina et al. 2011). This suggests that GMS may buffer these regions from even stronger precipitation shifts.

Fig. 10 shows the GMS response for the three greenhouse gas cases and their corresponding Eq. 7 estimates, Eq. 7 captures the qualitative behavior of GMS in the spatial pattern case: in the southern cell, slight decreases just south of the interior border most of the year and mild increases year-round south of $\sim$15°S and, in the northern cell, mild decreases most of the year. This behavior is essentially a (weakened) mirror image of the aerosol spatial pattern case, as the zonal mean surface temperature response increases (becomes more positive) nearly monotonically moving northward throughout the tropics.

The GMS responses to the full and uniform warming greenhouse gas cases are complicated, with Eq. 7 doing a poorer job than for the spatial pattern or for the three aerosol cases. In both northern and southern cells, GMS increases in some latitudes and months but decreases in others. This is in marked contrast to the theory, which predicts monotonically increasing GMS moving away from the ITCZ as discussed above. However, approximating GMS as the local upper (taken as 150 hPa) minus lower (925 hPa) level MSE – which does not appeal to the ITCZ arguments above – captures the full behavior much better than does Eq. 7 (not shown). Apparently, the ability of the ITCZ to set conditions throughout the tropics weakens in response to uniform warming. Note also that GMS response to the uniform warming and full greenhouse gas cases are the only fields analyzed featuring substantial variations between the two 8 year averaging subperiods mentioned previously.

4. Discussion

a. Gross moist stability changes near the ITCZ

Though both our theory and simulations indicate that GMS change is important near the cell centers, its behavior near the cells' interior border, in particular in the context of forced shifts of the ITCZ, is more subtle. As mentioned above, diagnosing the change in GMS in a finite resolution model becomes difficult near the Hadley cell interior boundary where both its numerator and denominator go to zero, with large unphysical dipoles occurring along the boundary.

Our theory for GMS change is well behaved computationally near the ITCZ, but assuming thermodynamic scaling of moisture seems suspect in the face of dynamical shifts of the ITCZ, as the necessary concurrent shift in moisture convergence will likely be a large term in the moisture budget. To the extent that $\Delta_{\mathrm{HC}} = 0$ at the ITCZ as we have assumed, an ITCZ shift necessarily implies a change in GMS over the latitudes over which the shift occurs: from a small positive value to zero at the new ITCZ position and from zero to a small positive value at the old position, for which the fractional GMS changes are respectively -100% and $+\infty$. This illustrates that the fractional change perspective of Eq. 3 becomes less useful – or equivalently that the mass flux and GMS are not easily separable – where the values become very small.

But provided the ITCZ does not move the theory remains appropriate at all tropical latitudes. Near the ITCZ, the scale of separation from the ITCZ is less than the meridional scales of variations in surface temperature change (Fig. 1(e,f)) and climatological surface specific humidity (not shown). Therefore the theory little GMS change at these latiudes in all runs (right columns of Figures 9 and 10). As a result, anomalous energy fluxes must manifest exclusively via anomalous circulation, which is consistent with the mass flux changes of large magnitude being confined to the latitudes near the ITCZ (Fig. 6).

A final caveat is the fact that the ITCZ and the cells interior border are not generally co-located, with the former generally displaced equatorward of the latter. Donohoe et al. (2013) note that this is a result of the maximum upward motion occurring where the meridional streamfunction gradient is largest, which for the large winter cell occurs equatorward of the streamfunction zero crossing. But definitionally the zero line of the computed GMS follows the $F_{\mathrm{HC}} = 0$ line (a.k.a. the "thermal equator"), while our theoretical estimate follows the ITCZ. Both results are conceptually self-consistent: the efficiency of energy transport is zero where the energy transport itself is zero, while the intense convection that communicates surface conditions most effectively to the free troposphere should be co-located with the maximum precipitation rates. However, the energy flux is poleward throughout either cell (e.g. Fig. 3(b)), and therefore GMS should be positive definite throughout, even at the ITCZ. Despite this conceptual shortcoming, the theory captures the qualitative behavior as discussed above.

b. *Connections to prior GMS studies*

The "stable get stabler" mechanism of GMS change we introduce is related to the "upped ante" mechanism of decreased precipitation at convective cell margins with global warming (Neelin et al. 2003; Chou and Neelin 2004), wherein increased surface moisture raises the "ante" for convection by increasing the boundary layer stability. From our perspective, this also enhances MSE aloft to an even greater extent than at the surface, thereby stabilizing the column and inhibiting convection. However, whereas the upped-ante mechanism is thought to act solely near the margins of convective zones – where moisture advection is sufficiently weak that the raised "ante" can not be met – our column stability mechanism holds at all latitudes away from the ITCZ.

In their detailed analysis of tropical precipitation response to global warming in CMIP3 models, Chou et al. (2009) note that the net change in GMS tends to be the residual of two large opposing factors. On the one hand, mean warming raises the tropopause and warms the free troposphere more than the surface, which act to increase the stability. On the other hand, the thermodynamically driven increase in moisture yields increased surface MSE, which destabilizes the column. From the perspective of our theory, the net stability change is best viewed not as a competition between the dry term aloft and moisture at the surface, but rather as between the surface temperature change locally and at the ITCZ acting on the climatological surface moisture field.

Importantly, this comparison with Chou et al. (2009) is somewhat apples-to-oranges, in that the GMS quantity they study is defined in terms of the vertical velocity profile $\Omega(p)$ at each latitude and longitude, in contrast to the meridional energy flux version we use. Additionally, they are concerned with the detailed energy and moisture budget changes at each location in order to understand the tropical precipitation response, while we are focusing on qualitative understanding of the large-scale energetic response. They demonstrate that in many locations dynamical changes can outweigh simple thermodynamic "rich-get-richer" behavior, which is consistent with the actual GMS behavior in our simulations being more complicated than our theory predicts and the above discussion of moisture convergence and ITCZ shifts.

c. Degree of symmetry between greenhouse gas and aerosol responses

While optimal fingerprinting techniques for detection and attribution of climate change to different forcing agents depend on well separable climate responses to those forcings, Xie et al. (2013) argue that the responses are, to the contrary, similar to one another due to inherent mechanisms of climate response that act symmetrically for a warming or cooling.

On the one hand, we find notable differences between the two forcing agents, including strong year-round northward energy and mass flux anomalies via the Hadley cells due to aerosols absent in the greenhouse gases case in the deep tropics. On the other hand, the overall GMS response to the spatial pattern components, the seasonality of Arctic temperature change, and some seasonal changes in the energy flux, mass flux, and GMS – namely the energy and mass flux changes in the NH winter cell, the extratropical energy flux year-round, and our theoretical estimate for GMS response to mean temperature change – are quite symmetric about zero.

There is some asymmetry between the mean temperature change cases of greenhouse gases vs. aerosols in some fields. Taken at face value, it suggests that the tropical meridional energy flux is nonlinear in mean surface temperature. Conversely, if the climate does in reality respond linearly to temperature perturbations in this range, this could be simply a deficiency of the AGCM. Pairs of simulation with equal magnitude and opposite signed uniform SST change would shed more light on this issue. As previously mentioned, Wyant et al. (2006) find asymmetric cloud radiative forcing responses in tropical ascent regions due to differing condensate changes in plus-2K vs. minus-2K experiments in AM2.1. Moreover, they attribute these changes to the Tokioka entrainment limiter paramater of AM2.1's convection scheme, and note that such asymmetry does not manifest in the NCAR CAM3.0 AGCM.

d. Prescibed SSTs

To the extent that the imposed SST anomalies induce an energetic imbalance that the atmospheric circulation at least partially compensates for, and to the extent that the imposed SST anomalies also govern the response of the gross moist stability based on our theoretical estimate, then the imposed SSTs have dictated both the energy flux and GMS responses. For the solsticial Hadley cell in which these are directly connected to the mass flux with eddy stresses playing little role, it follows that the forced mass flux response can be thought of as slaved to the energy and GMS forced responses (Merlis et al. 2013a). However, the degree of compensation by the atmosphere does not appear to be well constrained (Kang et al. 2008, 2009), and the gross moist stability in these simulations agrees only qualitatively with the the simple SST-mediated mechanisms that we have presented. Therefore, constraining the real world mass flux response to anthropogenic greenhouse gases and aerosols throughout the seasonal cycle – and with it the tropical precipitation response – remains a challenge.

Using prescribed SSTs is both vital and limiting. On the one hand, it enables the decomposition into mean and spatially varying components critical to understanding the model behavior. On the other hand, it prohibits coupling of the atmosphere and ocean responses that may be important in the real world. Additionally, Kang and Held (2012) demonstrate that model Hadley cell responses to extratropical forcing can be sensitive to the details of the imposed SST profiles, which could well stem at least in part from the GMS dependence on SSTs we have presented. We have not explored the sensitivity of the results to different SST patterns. SST anomalies were derived from simulations using a mixed-layer ocean-AGCM rather than a fully coupled atmosphere-ocean GCM, and prior studies have demonstrated important differences in the projected SST change with global warming between them, including the "enhanced equatorial response" in the tropical Pacific (e.g. Xie et al. 2010).

Timescale is another factor – the SST anomalies we use represent the equilibrium response of SM2.1, while the more immediately pressing issue from a societal perspective is the transient behavior.

Importantly, the mechanisms we have invoked to explain the GMS behavior act entirely through tropical SSTs, in particular the relative SST difference between a given latitude and at the ITCZ. In this sense, how efficiently the Hadley cell fluxes energy poleward as it overturns depends on the conditions in the extratropics only to the extent that they alter tropical SSTs. Yet in the summer and equinoctial cells it is well established that the mass flux is affected by stresses from extratropical eddies (e.g. Schneider 2006). Additionally, that the meridional energy flux depends on the equator to pole temperature gradient is a feature of both the classic angular momentum conserving axisymmetric model of the Hadley cells (Held and Hou 1980) and aquaplanet GCM simulations (e.g. Caballero and Langen 2005). How to reconcile these different aspects of the Hadley circulation is an open question.

5. Summary

Using the GFDL AM2.1 AGCM, we have explored how SST anomalies induced by historical anthropogenic emissions of either well-mixed greenhouse gases or aerosols affect the meridional transports of energy in the tropics throughout the annual cycle. Complementary simulations in which either the tropical mean SST anomaly was applied at all ocean gridpoints or the full SST anomalies minus this tropical mean was applied clarify the relative roles of the mean vs. the spatial pattern of SSTs.

Both forcing agents alter the net tropical meridional energy transport, its partitioning among the Hadley cells, stationary eddies, and transient eddies, and for the Hadley cells the relative roles of the mass flux and the gross moist stability. Greenhouse gases increase the poleward energy transport by eddies, an effect driven by the mean warming but somewhat negated by the polar amplified spatial pattern. Aerosols induce northward energy flux anomalies in the deep tropics via the Hadley cells due to their spatial pattern of the NH cooling relative to the SH; this feature is superimposed on a weakening of poleward energy transport due to the mean cooling.

The mass flux by the Hadley cells is weakened year-round by greenhouse gases, with contributions from both the tropical circulation slowdown mediated by the mean warming and the aforementioned weakened energy fluxes due to the polar amplification. For aerosols, southward mass flux anomalies for the surface branch occur year round in both NH and SH cells. This implies a spin down of the SH cell and spin up of the NH cell, both of which contribute to the northward energy flux that compensates for the imposed NH relative cooling. For both forcing agents, significant mass flux changes are confined to the latitude range bounded by the seasonal meridional migrations of the boundary between the two Hadley cells.

The Hadley cell gross moist stability, which indicates the efficiency with which the cells flux energy poleward as they overturn, thereby connecting the energy and mass fluxes, is equivalently a measure of the difference between upper and lower level moist static energies. By an argument set forth by Held (2001b) assuming that deep convection at the ITCZ homogenizes column MSE and that the weak temperature gradient constraint homogenizes MSE aloft in the horizontal, this is approximately equal to the difference between surface MSE values at the given latitude and at the ITCZ. An implication of this estimate combined with the Clausius-Clapeyron relation is that a uniform warming will tend to increase GMS moving meridionally away from the ITCZ, and conversely a uniform cooling will decrease it. Overlaid on this mechanism in the aerosol case is a reduction in GMS to the south of convection and an increase to the north due to the magnitude of cooling increasing nearly monotonically with latitude. This mechanism yields northward energy flux anomalies year round, thereby acting against the imposed NH cooling. This mechanism is also apparent in the greenhouse gases spatial pattern case, albeit with weaker magnitude and of opposite sign. Dynamical changes in moisture convergence associated with ITCZ shifts complicate the interpretation of our theory near the ITCZ, but nevertheless it predicts weak GMS change and thus may explain why the mass flux changes are strong at these latitudes.

We are encouraged by the insights engendered by these idealized SST perturbation experiments in comprehensive AGCMs. An added benefit is their fast integration time relative to fully coupled GCMs or earth system models. As mentioned previously, we view this work as a bridge between idealized aquaplanet simulations and fully coupled GCMs (or the real world) in which such a decomposition into mean and spatial pattern components is not feasible. How applicable the theoretical results we have presented are to the real world will hopefully be made clear by future analysis of fully coupled GCMs and observational data.

Acknowledgments.

We thank Leo Donner, Gabriel Lau, Tim Merlis, Dargan Frierson, Aaron Donohoe, Gabe Vecchi, and Jonathan Mitchell for insightful discussions. Two GFDL internal reviewers and two anonymous reviewers provided thoughtful reviews. S.A.H. was funded first by the NOAA/Princeton University Cooperative Institute for Climate Science and later by the Department of Defense National Defense Science and Engineering Graduate Fellowship.

APPENDIX

Calculation of meridional energy flux, mass flux, and gross moist stability

All experiments are integrated on the model's native sigma vertical coordinate system and then interpolated to regular pressure levels as monthly means for analysis. This interpolation produces a small imbalance (a few percent) between the zonal-mean northerly and southerly mass flows that result in somewhat noisy behavior when trying to compute the MSE flux explicitly by integrating MSE times the meridional flow. As such, we introduce an *ad hoc* correction by defining an adjusted zonal mean meridional wind,

$$[\overline{v}]_{\mathrm{adj}} \equiv [\overline{v}]_{+} + [\overline{v}]_{-}\frac{\{[\overline{v}]_{+}\}}{\{[\overline{v}]_{-}\}}, \tag{A1}$$

where $[\overline{v}]_{+}$ denotes southerly zonal mean wind (i.e. equal to $[\overline{v}]$ if $[\overline{v}] > 0$ and zero otherwise), $[\overline{v}]_{-}$ denotes northerly wind (defined conversely), and curly brackets denote a vertical mass-weighted integral, $\{\} \equiv \int \mathrm{d}p/g$, where the integral extends over the depth of the column. Note that $\{[\overline{v}]_{\mathrm{adj}}\} \equiv 0$, i.e. $[\overline{v}]_{\mathrm{adj}}$ is strictly in mass balance.

The mean meridional circulation component of the meridional MSE flux, i.e. the Hadley cell MSE flux $F_{\mathrm{HC}}(\phi)$, is computed using this mass flux adjusted wind:

$$F_{\mathrm{HC}}(\phi) = \int_{p_{\mathrm{top}}}^{p_{\mathrm{sfc}}} [\overline{m}][\overline{v}]_{\mathrm{adj}}\, \mathrm{d}p/g. \tag{A2}$$

The adjustment removes the interpolation-based noise (not shown), and the resulting MSE flux compares well with the inferred total atmospheric flux (defined below) in the deep tropics where the Hadley cells are expected to dominate the energy transport.

The stationary eddy component does not require any mass flux correction:

$$F_{\mathrm{st.\,edd.}}(\phi) = \int_{p_{\mathrm{top}}}^{p_{\mathrm{sfc}}} [\,\overline{m}^{*}\,\overline{v}^{*}\,]\, \mathrm{d}p/g. \tag{A3}$$

We infer the total atmospheric energy transport by assuming steady state and thus relating the total atmospheric energy flux divergence to the top-of-atmosphere (TOA) and surface flux difference: $\nabla \cdot F_m = Q_{\mathrm{TOA}} - Q_{\mathrm{sfc}}$, where subscripts refer to TOA and surface fluxes, respectively, with downward defined as positive. We then integrate zonally and meridionally:

$$F_{\mathrm{tot}}(\phi) = \int_{-\pi/2}^{\phi} \int_{0}^{2\pi} (Q_{\mathrm{TOA}} - Q_{\mathrm{sfc}}) a^2 \cos\phi \, \mathrm{d}\lambda \, \mathrm{d}\phi. \tag{A4}$$

The transient eddy term is then taken as the residual of the total minus the time mean (i.e. the Hadley cells plus stationary eddies): $F_{\mathrm{tr.\,edd.}}(\phi) = F_{\mathrm{tot}}(\phi) - F_{\mathrm{HC}}(\phi) - F_{\mathrm{st.\,edd}}(\phi)$. Because the total includes all energy while the explicit calculations include only moist static energy (neglecting kinetic energy), the transient eddy terms include any resulting residual. But presumably this residual term is small.

Another concern regarding the MSE flux by the Hadley Cells is the vertical extent of the integral. While all of our conceptual analysis invokes tropospheric circulation only, integrating to the model top includes stratospheric flow. Though this circulation is very weak and the densities very low, very large stability values due to the negative lapse rate and large MSE values due to the large geopotential term could result in non-negligible contributions to the net MSE flux. This could be especially relevant in AM3, a high-top model that extends vertically to 1 hPa, compared to 10 hPa for AM2.1. We test this effect by varying the vertical extent of the MSE flux integral (not shown). While the magnitude of the energy flux tends to reduce slightly by lowering the extent of the integral, the qualitative picture remains the same in either case.

There is also a clear downside to lowering the vertical integral for the Hadley cell or stationary eddy components. Since we are taking the transient eddy component as the residual of the total energy flux calculation – which implicitly includes the entire atmosphere – and the time mean component, moving the time mean integrals lower than the model top would lead to the transient eddy term being contaminated by the stratospheric time mean flow. For this reason we choose to integrate through the depth of the model atmosphere.

For the mass flux, we use the maximum magnitude value of the Eulerian meridional mass streamfunction at each latitude. The mass flux can also be obtained by integrating the adjusted meridional wind $[\overline{v}]_{\mathrm{adj}}$ from the surface to the level where the integral attains its maximum magnitude. The results in either case are nearly identical, and so we choose the former, it being more conventional and simpler to calculate.

We calculate the gross moist stability, Δ_{HC}, as the ratio of the energy flux by the Hadley cells, $F_{\mathrm{HC}}(\phi)$ to the mass flux, $\Psi_{\mathrm{max}}(\phi)$:

$$\Delta_{\mathrm{HC}}(\phi) \equiv \frac{\int_{p_{\mathrm{top}}}^{p_{\mathrm{sfc}}} [\overline{m}][\overline{v}]_{\mathrm{adj}} \, \mathrm{d}p/g}{\Psi_{\mathrm{max}}}. \tag{A5}$$

Thus defined, Δ_{HC} is positive for a thermally direct circulation such as the Hadley cells. In all plots of Δ_{HC} or its theoretical approximations, we divide by c_p as standard in order to get units of Kelvin.

REFERENCES

Boé, J., A. Hall, and X. Qu, 2009: Current GCMs' unrealistic negative feedback in the Arctic. *J. Climate*, **22 (17)**, 4682–4695, doi:10.1175/2009JCLI2885.1.

Bollasina, M. A., Y. Ming, and V. Ramaswamy, 2011: Anthropogenic aerosols and the weakening of the South Asian summer monsoon. *Science*, **334 (6055)**, 502–505, doi:10.1126/science.1204994.

Caballero, R. and P. L. Langen, 2005: The dynamic range of poleward energy transport in an atmospheric general circulation model. *Geophys. Res. Lett.*, **32 (2)**, L02 705, doi:10.1029/2004GL021581.

Chiang, J. C. H. and A. R. Friedman, 2012: Extratropical cooling, interhemispheric thermal gradients, and tropical climate change. *Ann. Rev. Earth. Planet. Sci.*, **40**, 383–412, doi:10.1146/annurev-earth-042711-105545.

Chou, C. and J. D. Neelin, 2004: Mechanisms of global warming impacts on regional tropical precipitation. *J. Climate*, **17 (13)**, 2688–2701.

Chou, C., J. D. Neelin, C.-A. Chen, and J.-Y. Tu, 2009: Evaluating the "rich-get-richer" mechanism in tropical precipitation change in global warming. *J. Climate*, **22**, 1982–2005, doi:10.1175/2008JCLI2471.1.

Chou, C., J. D. Neelin, U. Lohmann, and J. Feichter, 2005: Local and remote impacts of aerosol climate forcing on tropical precipitation. *J. Climate*, **18 (22)**, 4621–4636, doi:10.1175/JCLI3554.1.

Delworth, T. L., A. J. Broccoli, and co authors, 2006: GFDL's CM2 global coupled climate models. Part I: Formulation and simulation characteristics. *J. Climate*, **19 (5)**, 643–674, doi:10.1175/JCLI3629.1.

Dima, I. M. and J. M. Wallace, 2003: On the seasonality of the Hadley cell. *J. Atmos. Sci.*, **60 (12)**, 1522–1527.

Donohoe, A., J. Marshall, D. Ferreira, and D. Mcgee, 2013: The relationship between ITCZ location and cross equatorial atmospheric heat transport: From the seasonal cycle to the last glacial maximum. *J. Climate*, **26**, 3597–3618, doi:10.1175/JCLI-D-12-00467.1.

Frierson, D. M. W., 2007: The dynamics of idealized convection schemes and their effect on the zonally averaged tropical circulation. *J. Atmos. Sci.*, **64 (6)**, 1959–1976, doi:10.1175/JAS3935.1.

Frierson, D. M. W. and Y. T. Hwang, 2012: Extratropical influence on ITCZ shifts in slab ocean simulations of global warming. *J. Climate*, **25 (2)**, 720–733, doi:10.1175/JCLI-D-11-00116.1.

GFDL Atmospheric Model Development Team, 2004: The new GFDL global atmosphere and land model AM2-LM2: Evaluation with prescribed SST simulations. *J. Climate*, **17**, 4641–4673.

Held, I. M., 2001a: The general circulation of the atmosphere. *2000 Program in Geophysical Fluid Dynamics*, Woods Hole Oceanographic Institution, available at http://hdl.handle.net/1912/15.

Held, I. M., 2001b: The partitioning of the poleward energy transport between the tropical ocean and atmosphere. *J. Atmos. Sci.*, **58 (8)**, 943–948.

Held, I. M. and B. J. Hoskins, 1985: Large-scale eddies and the general circulation of the troposphere. *Advances in Geophysics*, **28A**, 3–31.

Held, I. M. and A. Y. Hou, 1980: Nonlinear axially symmetric circulations in a nearly inviscid atmosphere. *J, Atmos. Sci.*, **37 (3)**, 515–533.

Held, I. M. and B. J. Soden, 2006: Robust responses of the hydrological cycle to global warming. *J. Climate*, **19 (21)**, 5686–5699, doi:10.1175/JCLI3990.1.

Hwang, Y. T. and D. M. W. Frierson, 2010: Increasing atmospheric poleward energy transport with global warming. *Geophys. Res. Lett.*, **37 (24)**, L24 807, doi:10.1029/2010GL045440.

Kang, S. M., C. Deser, and L. M. Polvani, 2013: Uncertainty in climate change projections of the Hadley circulation: The role of internal variability. *J. Climate*, **26**, 7541–7554, doi:10.1175/JCLI-D-12-00788.1.

Kang, S. M., D. M. W. Frierson, and I. M. Held, 2009: The tropical response to extratropical thermal forcing in an idealized GCM: The importance of radiative feedbacks and convective parameterization. *J. Atmos. Sci.*, **66 (9)**, 2812–2827, doi:10.1175/2009JAS2924.1.

Kang, S. M. and I. M. Held, 2012: Tropical precipitation, SSTs and the surface energy budget: a zonally symmetric perspective. *Clim. Dyn.*, **38 (9-10)**, 1917–1924, doi:10.1007/s00382-011-1048-7.

Kang, S. M., I. M. Held, D. M. W. Frierson, and M. Zhao, 2008: The response of the ITCZ to extratropical thermal forcing: Idealized slab-ocean experiments with a GCM. *J. Climate*, **21 (14)**, 3521–3532, doi:10.1175/2007JCLI2146.1.

Lesins, G., T. J. Duck, and J. R. Drummond, 2012: Surface energy balance framework for arctic amplification of climate change. *J. Climate*, **25 (23)**, 8277–8288, doi:10.1175/JCLI-D-11-00711.1.

Ma, J. and S.-P. Xie, 2013: Regional patterns of sea surface temperature change: A source of uncertainty in future projections of precipitation and atmospheric circulation. *J. Climate*, **26**, 2482–2501, doi:10.1175/JCLI-D-12-00283.1.

Merlis, T. M., T. Schneider, S. Bordoni, and I. Eisenman, 2013a: Hadley circulation response to orbital precession: Part I: Aquaplanets. *J. Climate*, **26 (3)**, 740–753, doi:10.1175/2008JCLI-D-11-00716.1.

Merlis, T. M., T. Schneider, S. Bordoni, and I. Eisenman, 2013b: Hadley circulation response to orbital precession. Part II: Subtropical continent. *J. Climate*, **26 (3)**, 754–771.

Merlis, T. M., T. Schneider, S. Bordoni, and I. Eisenman, 2013c: The tropical precipitation response to orbital precession. *J. Climate*, **26 (6)**, 2010–2021, doi:10.1175/JCLI-D-12-00186.1.

Ming, Y. and V. Ramaswamy, 2009: Nonlinear climate and hydrological responses to aerosol effects. *J. Climate*, **22 (6)**, 1329–1339, doi:10.1175/2008JCLI2362.1.

Ming, Y. and V. Ramaswamy, 2011: A model investigation of aerosol-induced changes in tropical circulation. *J. Climate*, **24 (19)**, 5125–5133, doi:10.1175/2011JCLI4108.1.

Ming, Y., V. Ramaswamy, L. J. Donner, and V. T. J. Phillips, 2006: A new parameterization of cloud droplet activation applicable to general circulation models. *J. Atmos. Sci.*, **63**, 1348–1356, doi:10.1175/JAS3686.1.

Ming, Y., V. Ramaswamy, L. J. Donner, V. T. J. Phillips, S. A. Klein, P. A. Ginoux, and L. W. Horowitz, 2007: Modeling the interactions between aerosols and liquid water clouds with a self-consistent cloud scheme in a general circulation model. *J. Atmos. Sci.*, **64**, 1189–1209, doi:10.1175/JAS3874.1.

Neelin, J. D., C. Chou, and H. Su, 2003: Tropical drought regions in global warming and El Niño teleconnections. *Geophys. Res. Lett.*, **30 (24)**, 2275, doi:10.1029/2003GL018625.

Neelin, J. D. and I. M. Held, 1987: Modeling tropical convergence based on the moist static energy budget. *Monthly Weather Review*, **115 (1)**, 3–12.

Privé, N. C. and R. A. Plumb, 2007: Monsoon dynamics with interactive forcing. Part i: Axisymmetric studies. *J. Atmos. Sci.*, **64 (5)**, 1417–1430, doi:10.1175/JAS3916.1.

Rayner, N. A., D. E. Parker, E. B. Horton, C. K. Folland, L. V. Alexander, D. P. Rowell, E. C. Kent, and A. Kaplan, 2003: Global analyses of sea surface temperature, sea ice, and night marine air temperature since the late nineteenth century. *J. Geophys. Res.*, **108 (D14)**, doi:10.1029/2002JD002670.

Schneider, T., 2006: The general circulation of the atmosphere. *Annu. Rev. Earth Planet. Sci.*, **34**, 655–688, doi:10.1146/annurev.earth.34.031405.125144.

Sobel, A. H., J. Nilsson, and L. M. Polvani, 2001: The weak temperature gradient approximation and balanced tropical moisture waves. *J. Atmos. Sci.*, **58 (23)**, 3650–3665.

Trenberth, K. E. and D. P. Stepaniak, 2003: Covariability of components of poleward atmospheric energy transports on seasonal and interannual timescales. *J. Climate*, **16 (22)**, 3691–3705.

Vecchi, G. A. and B. J. Soden, 2007: Effect of remote sea surface temperature change on tropical cyclone potential intensity. *Nature*, **450 (7172)**, 1066–1070, doi:10.1038/nature06423.

Walker, C. C. and T. Schneider, 2006: Eddy influences on Hadley circulations: Simulations with an idealized GCM. *J. Atmos. Sci.*, **63 (12)**, 3333–3350, doi:10.1175/JAS3821.1.

Wyant, M. C., C. S. Bretherton, J. T. Bacmeister, J. T. Kiehl, I. M. Held, M. Zhao, S. A. Klein, and B. J. Soden, 2006: A comparison of low-latitude cloud properties and their response to climate change in three AGCMs sorted into regimes using mid-tropospheric vertical velocity. *Climate Dynamics*, **27**, 261–279, doi:10.1007/s00382-006-013804.

Xie, S.-P., C. Deser, G. A. Vecchi, J. Ma, H. Teng, and A. T. Wittenberg, 2010: Global warming pattern formation: Sea surface temperature and rainfall. *J. Climate*, **23 (4)**, 966–986, doi:10.1175/2009JCLI3329.1.

Xie, S.-P., B. Lu, and B. Xiang, 2013: Similar spatial patterns of climate responses to aerosol and greenhouse gas changes. *Nature Geoscience*, **6 (10)**, 828–832, doi:10.1038/ngeo1931.

List of Tables

Table 1. Annual mean surface air temperature anomaly (in K) for the global mean, the tropics (30°S–30°N), and the northern hemisphere minus the southern hemisphere in the full, mean, and spatial pattern simulations for greenhouse gases and aerosols.

	Globe	Tropics	NH–SH
Greenhouse gases			
Full	2.6	2.3	0.3
Mean	2.3	2.3	0.1
Spatial pattern	0.1	−0.1	0.2
Aerosols			
Full	−1.6	−1.3	−0.9
Mean	−1.3	−1.3	−0.1
Spatial pattern	−0.3	−0.1	−0.7

Table 2. Columns from left to right: month, the latitude of the maximum magnitude of the mass streamfunction (in degrees and denoted ϕ_{max}) in the control simulation, the northward MSE flux by the Hadley cell at the latitude ϕ_{max} in the control simulation (in PW), and the fractional changes in the full aerosols simulation from the control at ϕ_{max} of the Hadley cell energy flux, mass flux, and gross moist stability. The months begin in April rather than January so that the periods when the southern hemisphere (April to October) or northern hemisphere (November to March) cell are strongest are each continuous within the table.

Month	ϕ_{max}	$F_{\text{MMC}}(\phi_{\text{max}})$	$\frac{\delta F_{\text{MMC}}}{F_{\text{MMC}}}(\phi_{\text{max}})$	$\frac{\delta \Psi_{\text{max}}}{\Psi_{\text{max}}}(\phi_{\text{max}})$	$\frac{\delta \Delta_{\text{HC}}}{\Delta_{\text{HC}}}(\phi_{\text{max}})$
4	-13.1	-1.12	-0.14	-0.02	-0.11
5	-9.1	-1.68	-0.20	-0.07	-0.14
6	-5.1	-2.21	-0.27	-0.13	-0.17
7	-5.1	-2.71	-0.21	-0.07	-0.14
8	-5.1	-2.65	-0.17	-0.07	-0.11
9	-5.1	-2.19	-0.23	-0.08	-0.17
10	-7.1	-1.12	-0.32	-0.07	-0.26
11	15.2	1.80	0.10	0.09	0.01
12	11.1	2.09	0.21	0.17	0.03
1	9.1	2.53	0.22	0.16	0.05
2	7.1	2.19	0.20	0.15	0.04
3	9.1	1.48	0.28	0.16	0.10

List of Figures

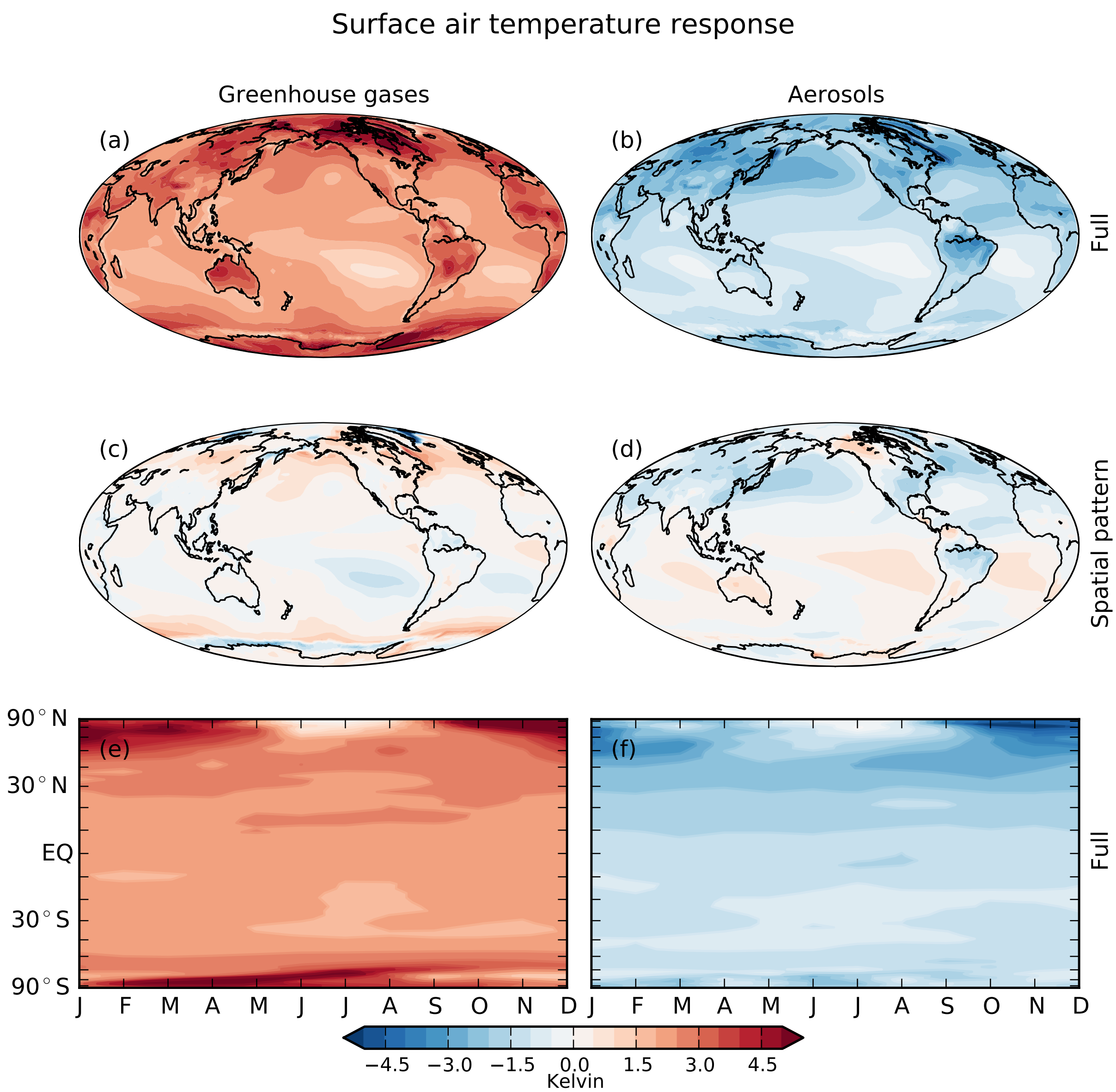

Fig. 1. Surface air temperature response for the prescribed SST experiments: annual mean for (a) greenhouse gases, (b) aerosols, (c) greenhouse gases spatial pattern, and (d) aerosols spatial pattern, and the annual cycle of their zonal mean for (e) greenhouse gases and (f) aerosols. The vertical axis in panels (e) and (f) is $\sin\phi$ to be proportional to Earth's fractional surface area at each latitude.

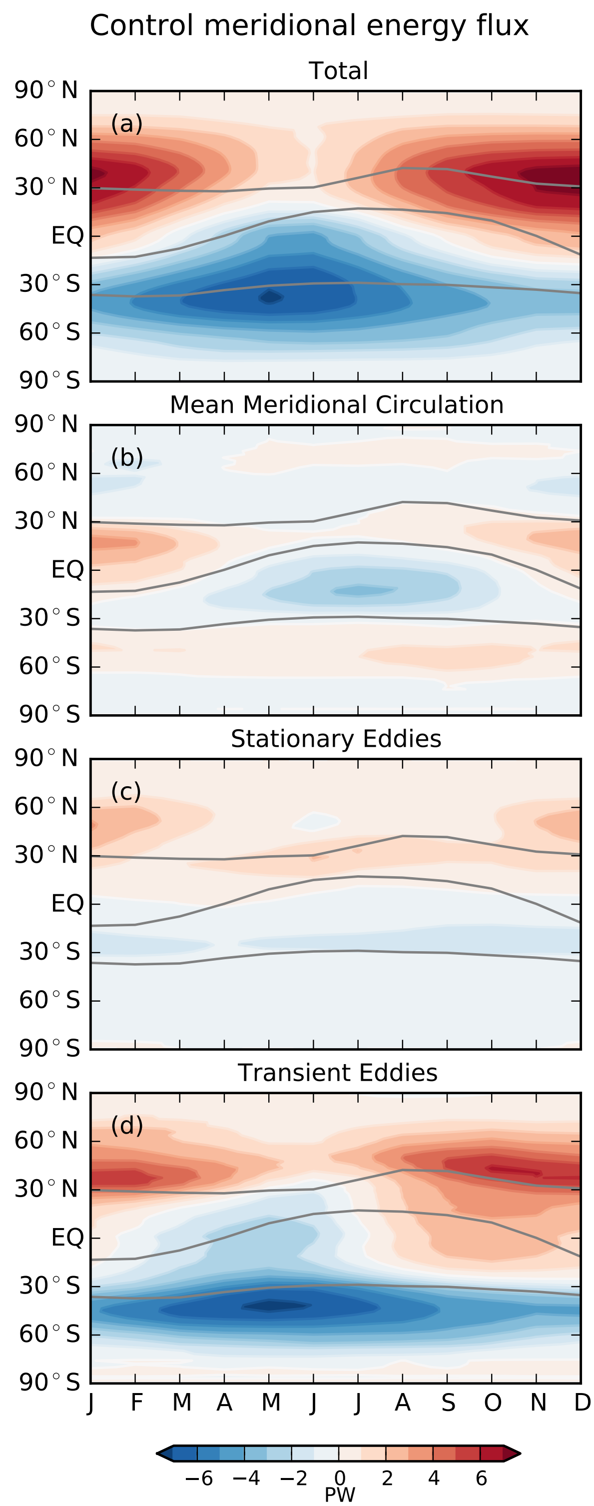

Fig. 2. Annual cycle of northward energy flux in the prescribed SST control simulation in color contours: (a) its total, and contributions from (b) the mean meridional circulation, (c) stationary eddies, and (d) transient eddies. Grey curves denote the positions of the Hadley cells' poleward boundaries and their shared interior border as defined by the zero crossings of the meridional mass streamfunction at 500 hPa. Because the flux calculations incorporate the surface area, no $\cos\phi$ spacing is necessary on the vertical axis.

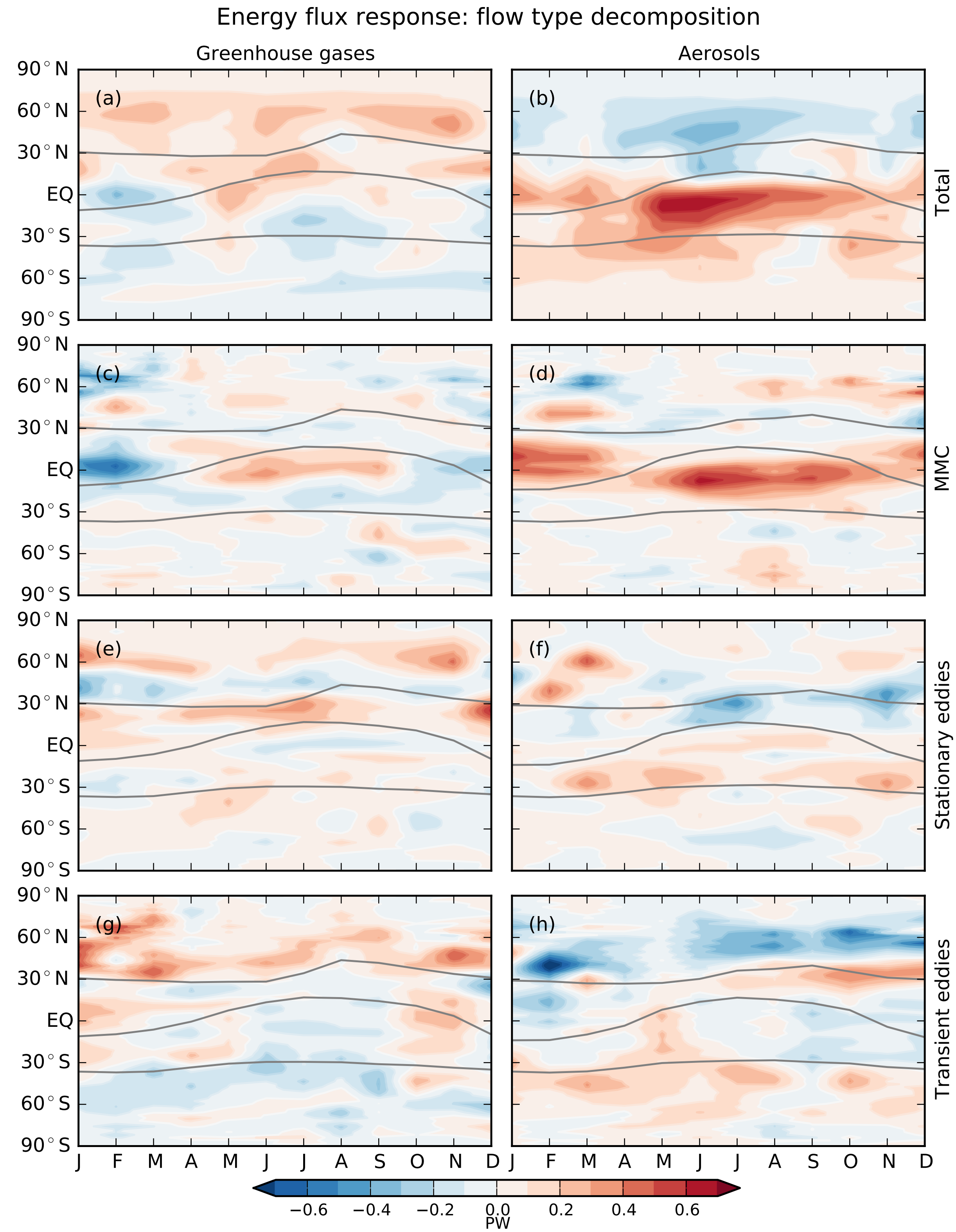

FIG. 3. Annual cycle of the anomalous northward atmospheric energy transport for the three (left column) greenhouse gas and (right column) aerosol simulations, (a,b) in total and by each flow component: (c,d) the mean meridional circulation, (e,f) stationary eddies, and (g,h) transient eddies. Overlaid grey curves mark the locations of the Hadley cells' poleward boundaries and their shared interior border in the perturbation simulation as defined by the zero crossings of the meridional mass streamfunction at 500 hPa.

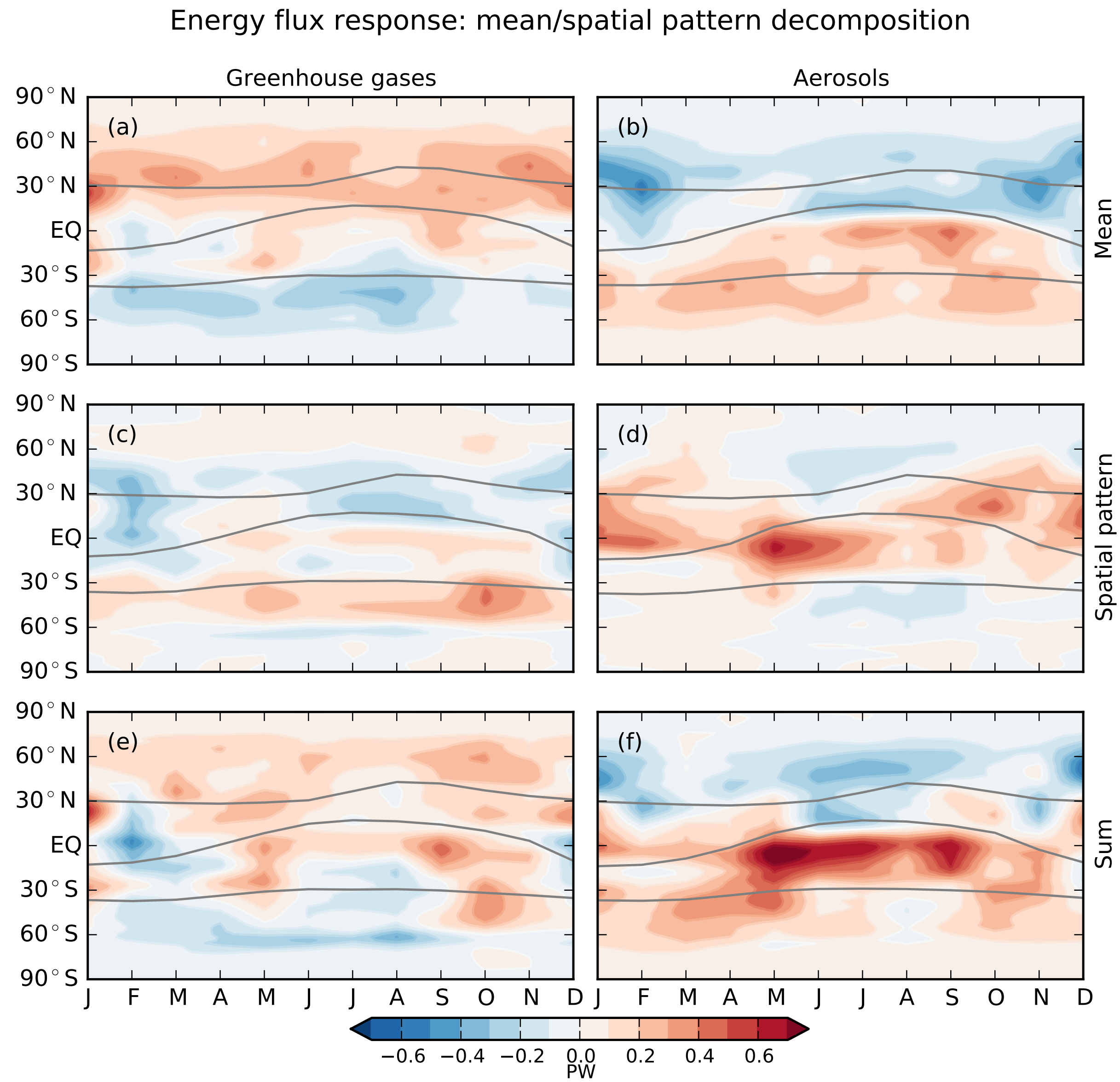

FIG. 4. As in Fig. 3, but for anomalous total northward atmospheric energy transport as defined by Eq. A4 for the (top row) uniform temperature change, (center row) spatial pattern cases and (bottom row) their sum. The grey curves denote the Hadley cell borders in the perturbation simulation as in Fig 3 for (a)-(d) and the average of their values in the uniform and spatial pattern cases for (e) and (f).

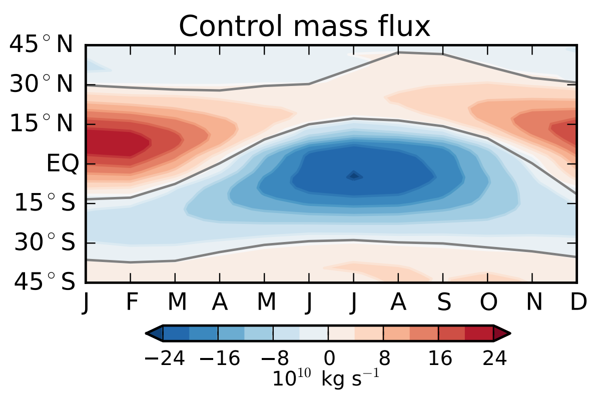

FIG. 5. Annual cycle of the mass flux, $\Psi_{\max}$, in the control simulation for 45°S-45°N, defined as the signed maximum magnitude of the meridional mass streamfunction at each latitude, where the streamfunction Ψ is defined as standard by Eq. 4. Positive values, as in the NH cell, denote northward flow in the upper branch of the overturning circulation. Overlaid grey curves denote the boundaries of the Hadley cells defined based on the zero crossings of Ψ at 500 hPa.

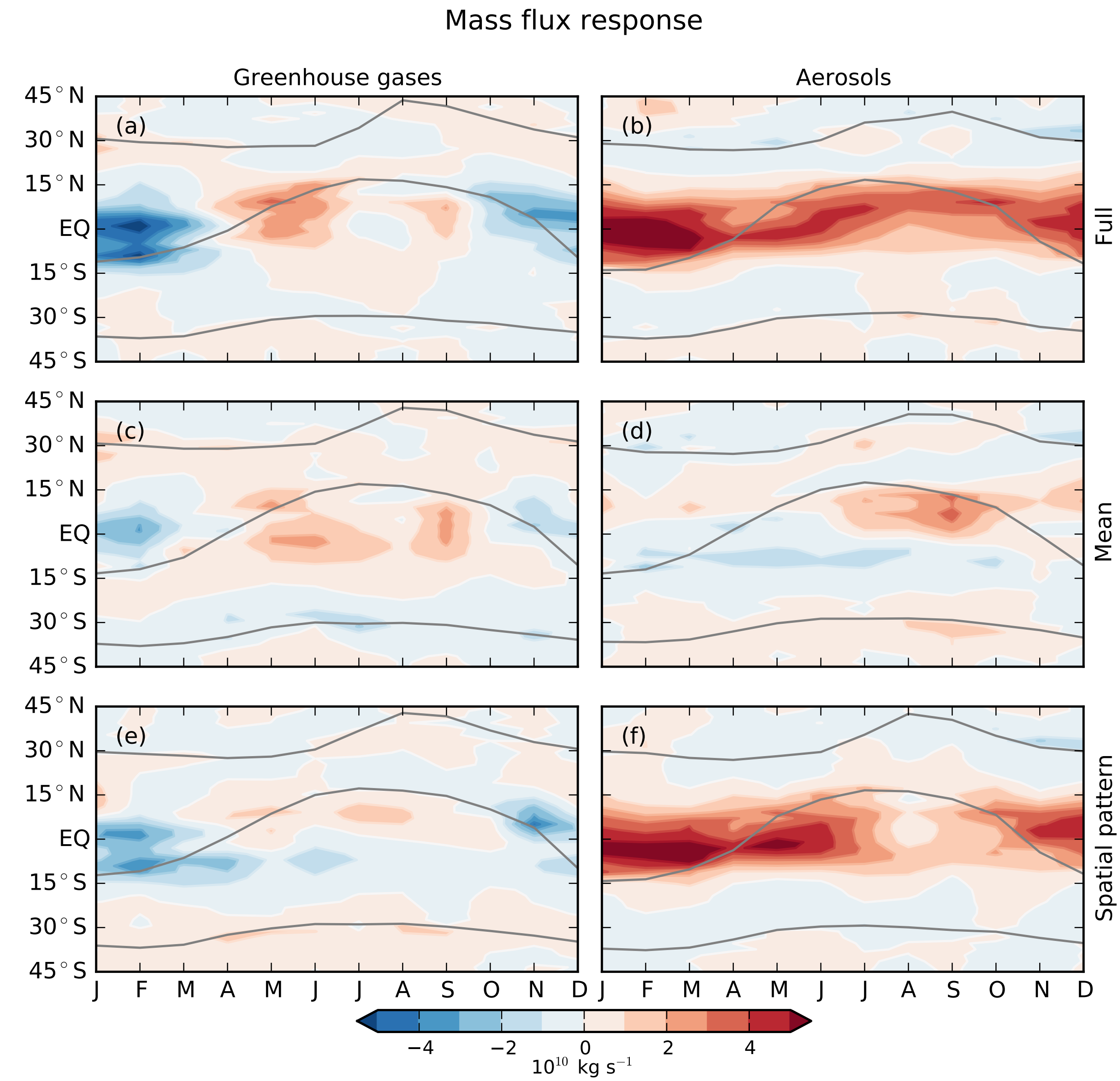

FIG. 6. Annual cycle of the mass flux response for 45°S-45°N in the (left column) greenhouse gas and (right column) aerosol (top row) full, (middle row) uniform temperature change, and (bottom row) spatial pattern cases.

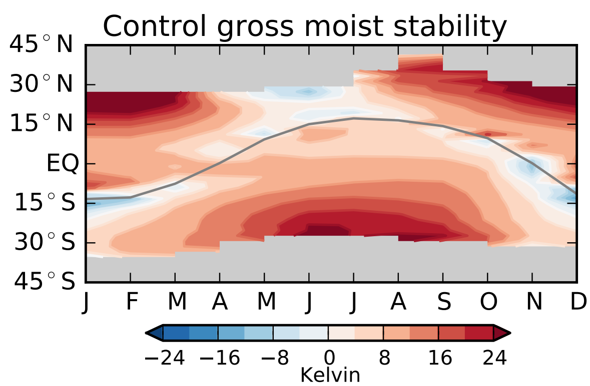

FIG. 7. Annual cycle of gross moist stability $\Delta_{\mathrm{HC}}(\phi)$ in the control simulation. Positive values indicate a thermally direct circulation, i.e. that the net meridional energy flux is in the same direction as the flow in the upper branch, as occurs in the Hadley cells . Values outside the Hadley cells are masked, as the primary concern is with tropical energy fluxes and since the underlying dynamics differ markedly for the Hadley and Ferrel cells. GMS has been divided by c_p in this and all subsequent plots as standard to get units of Kelvin.

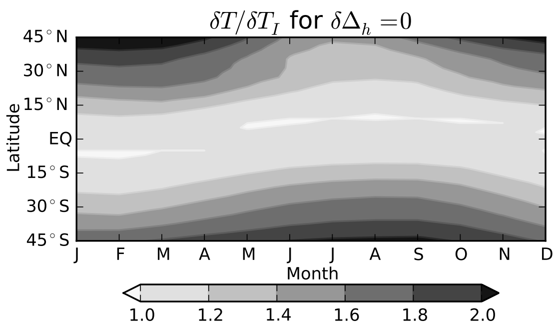

FIG. 8. Ratio of near-surface temperature change at the given latitude and at the intertropical convergence zone (ITCZ) necessary for GMS change to be zero. Based on Eq. 8 using 925 hPa values of q and T taken from the control simulation. The ITCZ latitude is taken as the latitude of maximum zonal mean precipitation, linearly interpolated between model grid points to where $\partial P/\partial \phi = 0$.

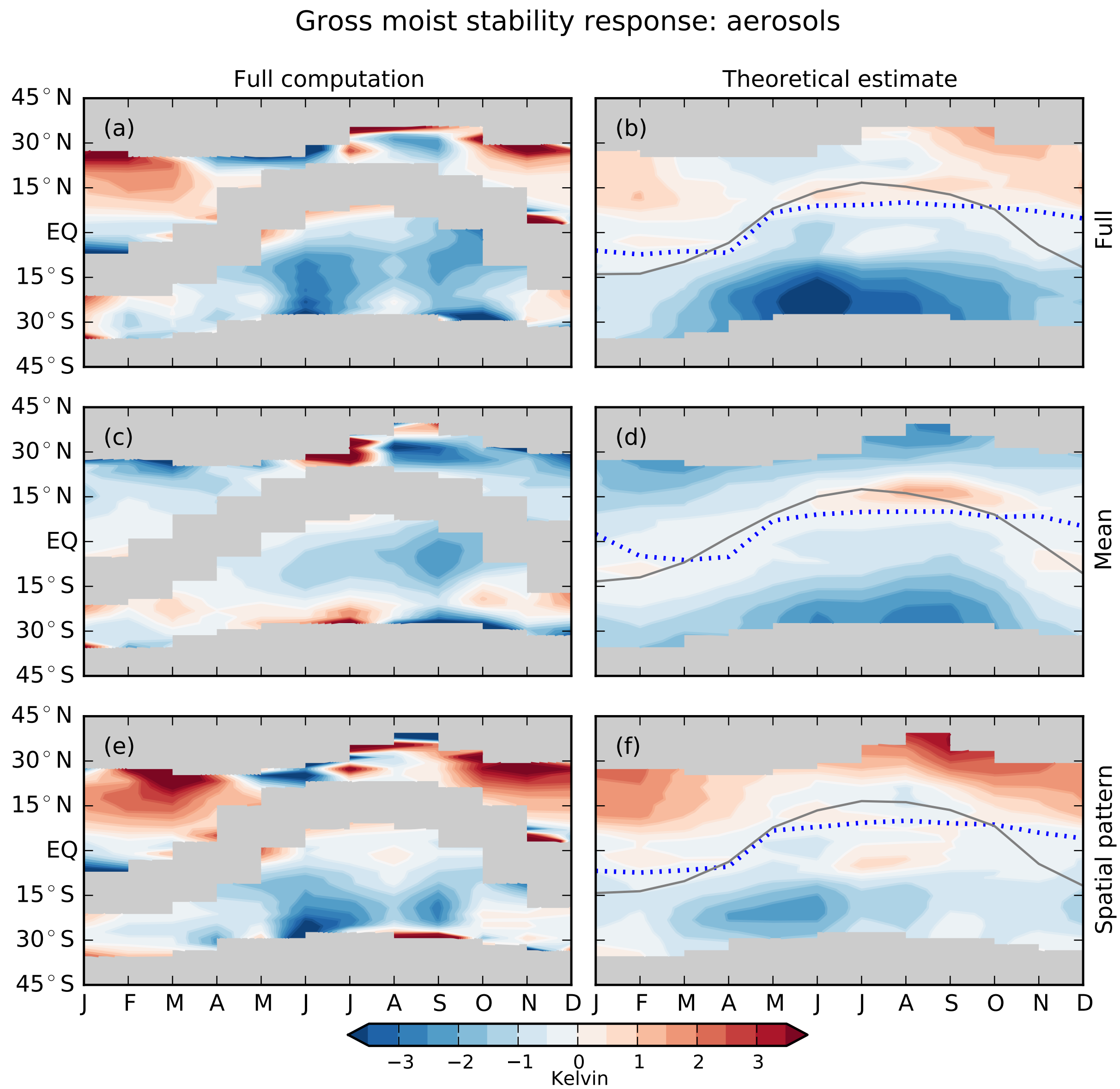

FIG. 9. Annual cycle of the gross moist stability response to the aerosol (top row) full, (middle row) uniform temperature change, and (bottom row) spatial pattern cases, as computed using (left column) the full GMS calculation of Eq. A5 and (right column) the theoretical estimate Eq. 7. Values outside the Hadley cells are masked in all panels, and values within 6° latitude of the Hadley cells' interior border on either side are also masked out in the left column, as the GMS calculation becomes problematic near where the mass flux goes to zero.

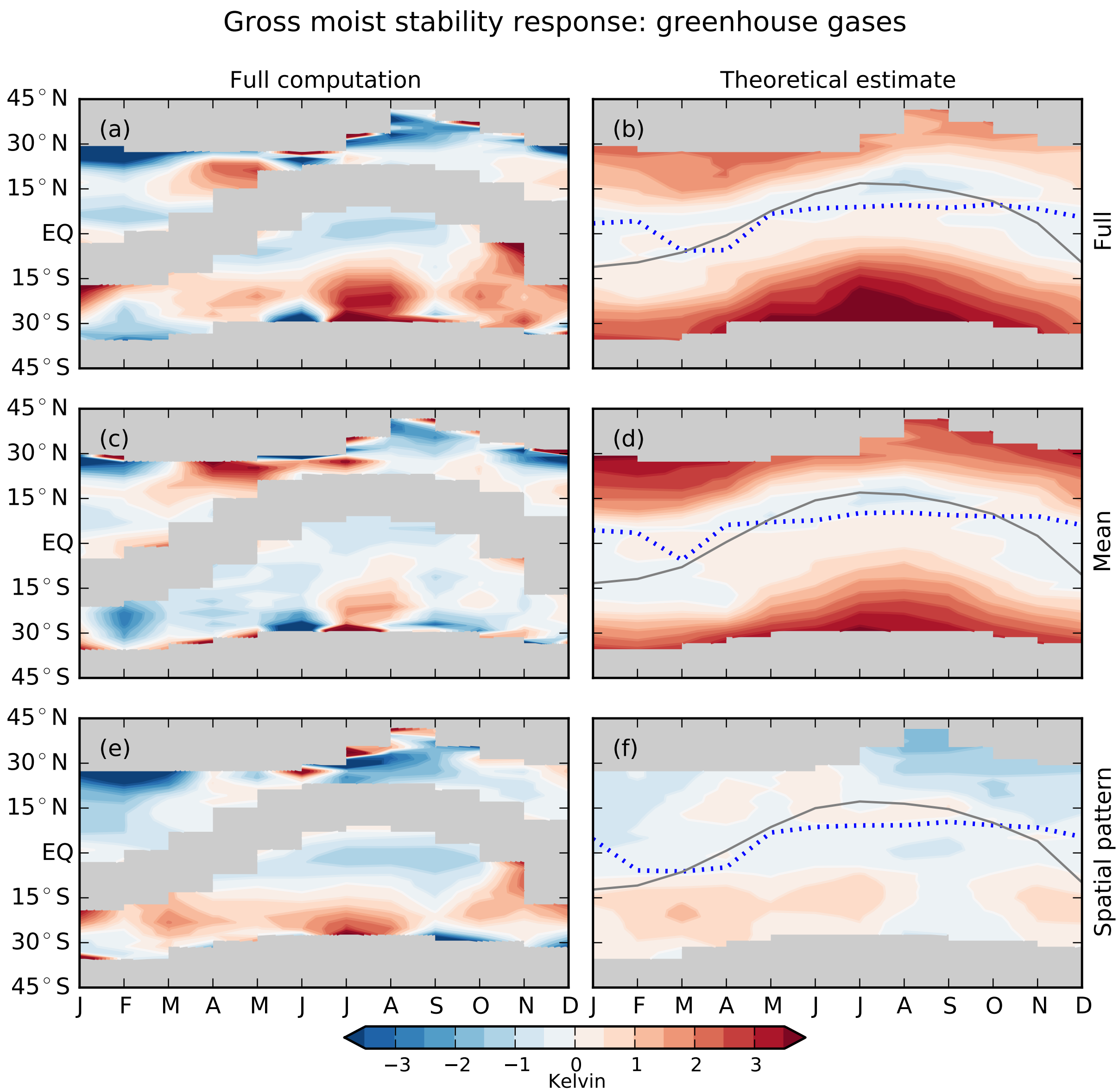

FIG. 10. As in Fig. 9, but for the greenhouse gas simulations.